PIER M

(Received 4 December 2023, Accepted 18 January 2024, Scheduled 2 February 2024)

Dual-Band and Dual-Sense Circularly Polarized Dielectric Resonator Antenna with Filtering Response

Chuanyun Wang, Weikang Hu*, Xiaofeng Jiang, Qilei Fan, and Jianjun Huang

School of Information Engineering, East China Jiaotong University, Nanchang 330013, China

ABSTRACT: A dual-band dual-sense (DBDS) circularly polarized (CP) filtering dielectric resonator antenna (FDRA) with a quasi-elliptic band-pass response is proposed in this paper. The proposed antenna consists of a rectangular dielectric resonator (DR) with a Z-shaped strip at the top, a ground plane with a rectangular slot, and a microstrip feedline etched with a section of the spur line. By using the microstrip coupled slot line structure to excite DR with a Z-shaped strip, different senses of circular polarization are achieved in the two bands. The results show that the lower and upper bands are independently controlled by the strip and the DR, respectively. In addition, three radiation nulls are generated at the passband's edge by elaborately designing a half-wavelength open stub and etching the spur line. For demonstration, a prototype DBDS CPFDRA is fabricated and measured. The measurements illustrate that the antenna achieves a wide impedance bandwidth of 38.2%, as well as a dual axial ratio (AR) bandwidth of 2.2% for the left-hand circular polarization (LHCP) and 4% for the right-hand circular polarization (RHCP). The realized gain exhibits a decline of 25 dB at the passband edge, indicating high selectivity.

1. INTRODUCTION

Linearly polarized (LP) or circularly polarized (CP) antennas have been developed over the years. The latter possess ideal characteristics, such as reducing multipath interference, fading effects, and minimizing polarization mismatch between transmitting and receiving antennas. CP antennas have been extensively studied and applied in the fifth generation (5G) mobile communication systems [1]. Dielectric resonator antennas (DRAs) have garnered significant attention due to their inherent advantages of low cost, low profile, and wide/multi-band impedance characteristics [2].

Circularly polarized dielectric resonator antennas (CPDRAs) can be excited through a single feed or multiple feeds. Although multi-feed technology can achieve a wider bandwidth than a single feed, it often necessitates an additional feed network, such as hybrid couplers and Wilkinson power divider, which undoubtedly increases antenna size and insertion loss. In modern wireless systems, efficient and compact antennas are preferred. Consequently, the realization of CPDRAs through a single feed has become a recent research focus [3–5]. Nonetheless, the majority of research articles on CP antennas are limited to single-band operation. Dual-band technology has garnered widespread attention due to its potential to significantly reduce the capacity and system cost of wireless communication systems [6–9]. The dual-band CP effect can be achieved by placing a pair of orthogonally positioned DRs over a planar "I"-shaped monopole [6]. The CP of the two bands is generated in [7] by introducing two orthogonal bands of perturbation into the center space of the outer and inner rings. The stacked structure design [8, 9] also demonstrates good dual-band CP performance. To enhance channel isolation between dual bands, suitable for modern wireless communication systems, the concept of dual-sensing (opposite polarization mode) performance was introduced for dual-band CPDRAs [10–14]. The traditional narrow-slot radiator is reshaped in [11] to establish two pairs of orthogonal polarizations with opposite rotations using three resonant modes (λ mode and 0.5λ mode) and (0.5λ mode and 2λ mode). The three modes are then reconfigured at the resonant frequency and sequentially excited in the rotation of the specified λ, 0.5λ, and 2λ modes. In addition, the asymmetric Swastik-shaped aperture coupling of the cylindrical DRA can also achieve a dual-band double-sensing (DBDS) effect [12], although the antenna's bandwidth cannot be individually controlled. In [13], a butterfly dielectric resonator is excited by an L-shaped slot and a vertical metal strip to achieve a wide dual-sense CP bandwidth. However, this structure is challenging to fabricate, and the out-of-band suppression level is not significant, as discussed in the above literature.

To achieve a multi-function antenna with miniaturization and improved mitigation of out-of-band interference, the concept of the filter dielectric resonator antenna (FDRA) has sparked extensive and fervent discussions [15–17]. For instance, the co-design method in [15] employs a band-pass filter as the feed network of the DRA to achieve filtering effects. The filtering function is implemented through a slot line stepped-impedance resonator (SSIR) slot structure [16]. Presently, most filter antennas focus on LP, with only a few achieving CP filtering effects [18–20]. In [19], a patch radiator is excited by integrating a power divider and a bandpass filter in the microstrip feedline to realize a filtered CP antenna. However, due to the integration of multiple components, the antenna size is not compact.

* Corresponding author: Weikang Hu (weikanghu0125@163.com).

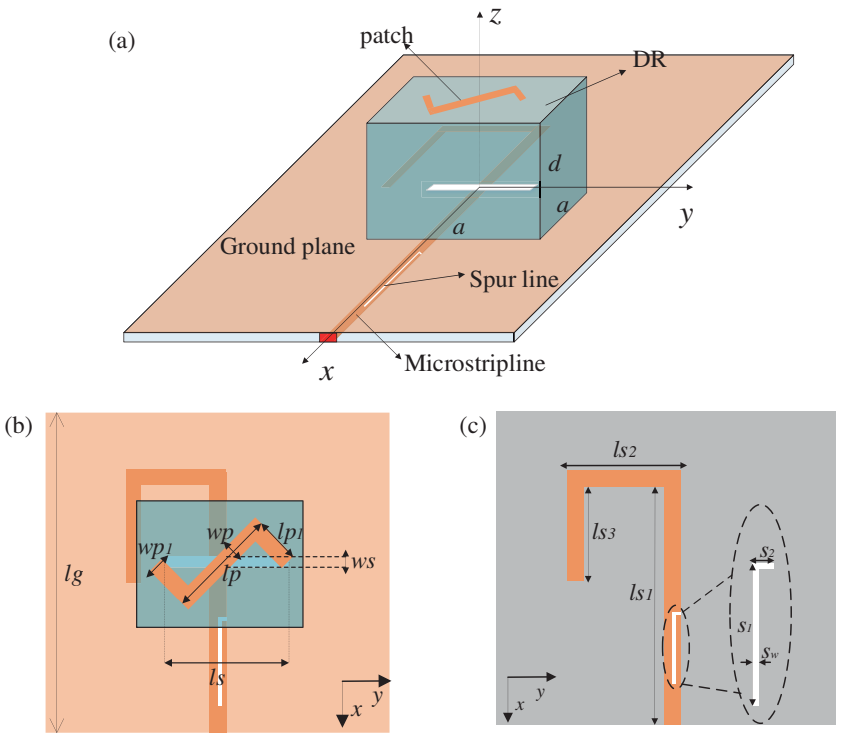

FIGURE 1. Configuration of the proposed DRA. (a) Perspective view; (b) Top view; (c) Bottom view.

Achieving such a high level of integration is challenging, as several design criteria need to be simultaneously met, including return loss, axial ratio (AR), radiation mode, and out-of-band suppression. Therefore, integrating filtering functions into CP antennas remains a significant challenge.

To effectively address these issues, this paper proposes a DBDS CPFDRA with quasi-elliptic bandpass response. RHCP is realized at high frequency by introducing a Z-shaped strip to disturb the DR electric field, while LHCP is achieved at low frequency due to the strip's inherent resonance. Notably, the low and high-frequency bands can be independently controlled by the strip and the DR, respectively. To improve the out-of-band selectivity a radiation null is introduced at high frequency by etching the spur line on the feedline, and a half-wavelength open stub is designed to introduce a radiation null at low frequency. The frequency doubling effect produces an additional null at the high frequency, contributing to high out-of-band selectivity. Hence, there is no need for any extra filtering circuit to achieve efficient filtering and radiation performance, and the construction is highly compact. As a result, this paper presents a DBDS CPFDRA with individually controllable CP frequency bands and quasi-elliptic bandpass response.

2. ANTENNA DESIGN

2.1. Antenna Configuration

Figure 1 illustrates the structure of the proposed DBDS CPFDRA. It primarily comprises a substrate, a DR with a Z-shape strip (the Z-shape strip is rotated 45° counterclockwise relative to DR), and a microstrip-slot coupled feed structure. The rectangular DRA with a relative permittivity of $\varepsilon_{r1} = 10$ is located over the ground. The microstrip feedline is fabricated on FR4 substrate with a relative permittivity of $\varepsilon_{r2} = 4.4$, and a thickness of $h = 0.762$ mm. The Z-shaped strip serves a dual purpose: it transforms the DRA mode of the LP field into a CP field as a perturbation structure and facilitates CP at low frequency through rectangular slot excitation, thereby achieving DBDS operation. To achieve miniaturization, reduced out-of-band interference, and multi-functional effect, the microstrip feedline incorporates an intricately designed open stub and a spur line. The design results in the generation of three radiation nulls on either side of the passband. The specific antenna parameters are presented in Table 1. The proposed antenna is simulated and optimized by Ansys high-frequency structure simulator (HFSS).

2.2. Operating Principle

To elucidate the operation of the proposed DBDS CPFDRA, we explain the antenna's working principle by comparing it with three reference antennas. The configuration of the reference antennas is shown in Fig. 2: 1) a microstrip line coupled rectangular slot-fed DRA; 2) the DR atop antenna I is loaded with a Z-shaped strip; 3) etching of the spur line on the microstrip feedline; and 4) for comparison, the proposed antenna featuring a meticulously designed half-wavelength open stub is also shown in Fig. 2(d). Fig. 3 presents the corresponding reflection coefficient, realized gain, and axial ratio for the DRAs with distinct structures. The reference antenna 1 is the original DRA fed by a 50 Ω microstrip wire through a slot etched into the ground plane. From the dielectric waveguide model (DWM) model [21],

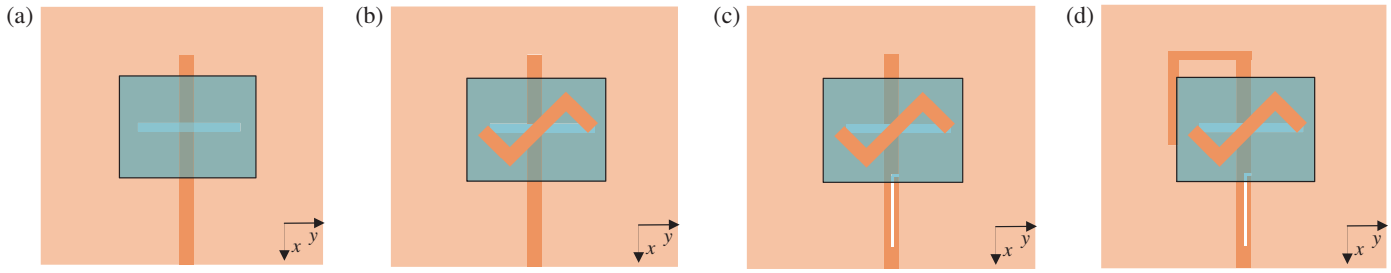

FIGURE 2. Antenna configurations (a) Reference antenna I: microstrip-line coupled rectangular slot fed DRA. (b) Reference antenna II: based on antenna I, the top of DR is covered with a Z-shaped strip. (c) Reference antenna III: etching the spur line on the microstrip feedline. (d) Proposed antenna: carefully designed half-wavelength open stub.

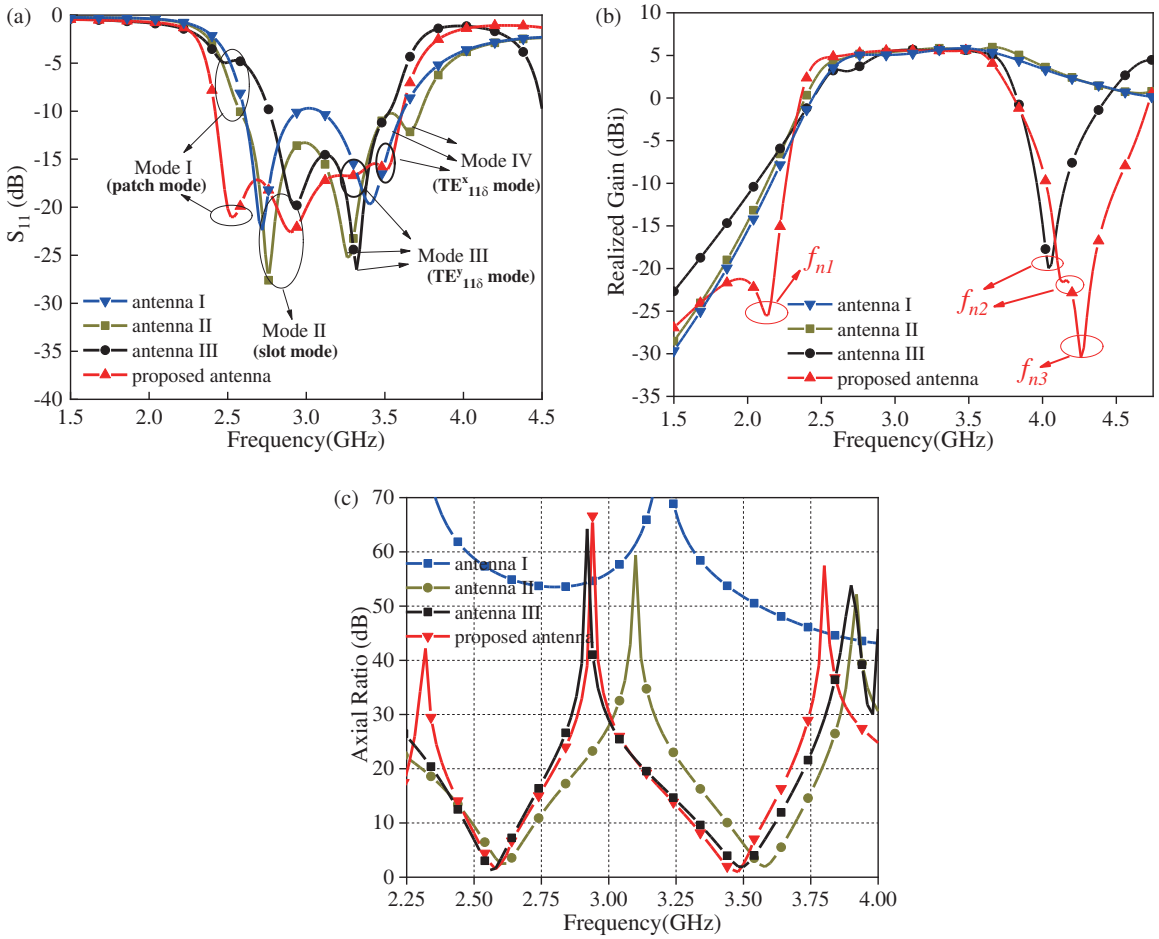

FIGURE 3. Simulated reflection coefficients, boresight gains, and Axial Ratio of the reference and proposed antennas. (a) Reflection coefficient. (b) Realized gain. (c) Axial Ratio.

the resonant frequency of DR is given by the following formula:

$$f_o = \frac{c}{2\pi\sqrt{\varepsilon_r}}\sqrt{k_x^2 + k_{\mathrm{y}}^2 + k_z^2} \tag{1}$$

$$k_x = \frac{\pi}{a} \tag{2}$$

$$k_z = \frac{\pi}{2d} \tag{3}$$

$$k_y = \sqrt{k^2 + k_x^2 + k_z^2} \tag{4}$$

where f_o represents the resonant frequency of $\mathrm{TE}^{\mathrm{y}}_{11\delta}$ mode.

The initial length of the Z-shape strip is set to half a wavelength at the resonant point, and its total length can be given by the following formula [22].

$$L = \frac{c}{2f\sqrt{\varepsilon_e}} - 2\Delta L \tag{5}$$

$$\Delta L = 0.412h\frac{(\varepsilon_e + 0.3)(W/h + 0.264)}{(\varepsilon_e - 0.258)(W/h + 0.8)} \tag{6}$$

TABLE 1. Main design parameters of antenna (Unit: mm).

lg	a	b	d	h	lp	lp_1	wp	wp_1
40	20.8	20.8	16.4	0.762	12.9	4.5	1.9	2
s_1	s_2	sw	ls_1	ls_2	ls_3	ls	ws	
10.5	0.5	0.2	17.3	13.3	9.1	16.4	1.6	

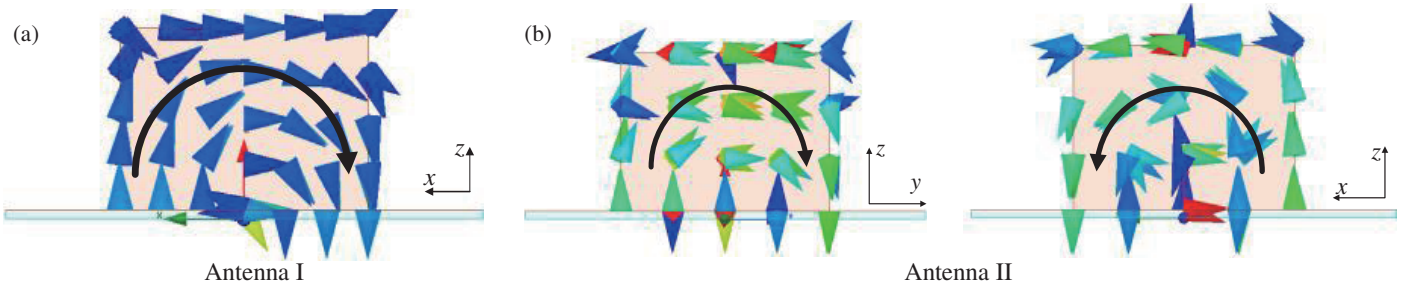

FIGURE 4. DR electric field distribution. (a) 3.5 GHz. (b) 3.3 GHz, 3.66 GHz.

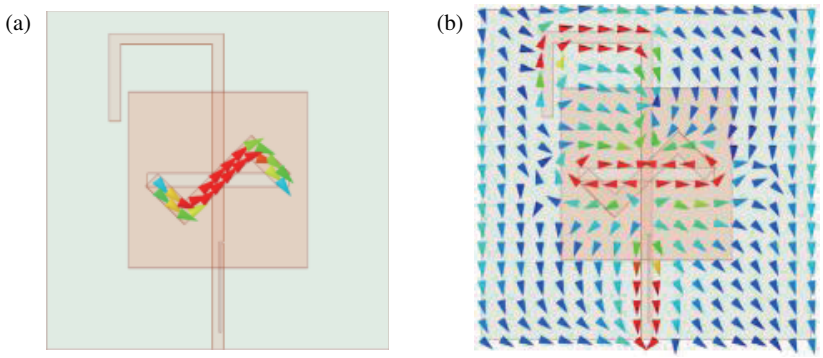

FIGURE 5. Strip and slot current distribution. (a) 2.54 GHz. (b) 2.9 GHz.

$$\varepsilon_e = \frac{\varepsilon_r + 1}{2} + \frac{\varepsilon_r - 1}{2}\left[1 + 12\frac{h}{W}\right]^{-1/2} \tag{7}$$

where L, ε_e, and ΔL represent the total length of the Z-shaped microstrip, the effective dielectric constant, and the equivalent radiation gap length, respectively.

From the figures, it becomes evident that antenna I has only two resonant modes (corresponding slot mode [23] and $\mathrm{TE}^{\mathrm{x}}_{11\delta}$ mode) within the passband, with poor edge selectivity on both passband sides. Moreover, as observed from the AR diagram, the polarization is LP characteristics. Upon introducing a Z-shape strip at the top of the DR in antenna I as shown in Fig. 3(c), two frequency bands achieve achieve circular polarization characteristics. The Z-shaped strip serves a dual purpose: it acts as a perturbation structure converting the DRA mode of the LP field into the RHCP field (with the strip field positioned 135° counterclockwise to the DR field) and stimulates the LHCP field mode of the strip through the slot line (with the slot line field positioned 45° clockwise to the strip field). As depicted in Fig. 4, when driven by a traditional rectangular slot, the mode stimulated by the DR is the $\mathrm{TE}^{\mathrm{x}}_{11\delta}$ mode, incapable of realizing circular polarization. However, with the introduction of a Z-shaped strip in antenna I, the strip disrupts the electric field distribution of the DR, splitting the fundamental mode into $\mathrm{TE}_{11\delta}$ modes along both Y and X directions, successfully achieving RHCP for the DR. Simultaneously, as showing in Fig. 5, the electric field of the strip and slot decomposes into clockwise rotation, yielding LHCP. This enables the realization of CP fields with opposite polarizations at both low and high frequencies. When the strip is oriented clockwise, an opposite circular polarization state is obtained.

However, the out-of-band selectivity remains inadequate. To enhance suppression at high frequencies, antenna III introduces a radiation null (f_{n2}) at high frequency by etching a spur line on the feedline. At f_{n2}, energy is concentrated near the spur line and no energy is coupled to the slot line to produce a radiating zero. However, the out-of-band selectivity at low frequencies remains suboptimal. To enhance rejection performance at low frequency, our proposed antenna is elaborately designed to incorporate a half wavelength stub at the f_{n1} of the low-frequency null beyond the rectangular slot section. The microstrip line is open at the end. It becomes zero after moving an integer distance of half a wavelength, so no signal can be coupled into the slot, producing a radiating null. Notably, a radiating null (f_{n3}) emerges at high frequency due to the frequency doubling effect. In order to better understand the three radiation nulls generated

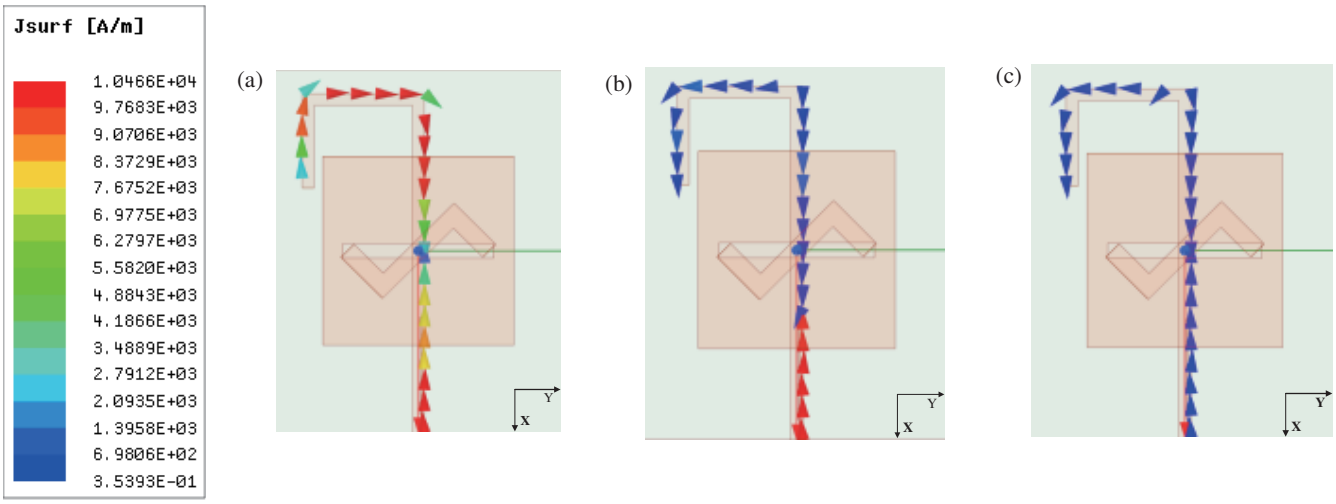

FIGURE 6. Simulated current of the proposed DRA at null frequencies. (a) 2.16 GHz. (b) 4.14 GHz. (c) 4.3 GHz.

by the lower and upper edges of the antenna passband, the simulated current distribution is shown in Fig. 6. Fine-tuning of the antenna's structural parameters is performed to achieve optimal impedance matching. An out-of-band suppression level greater than 25 dB is obtained in the stopband, and the quasi-elliptic band-pass filtering response is realized.

2.3. Parameter Analysis

To validate the proposed DBDS CPFDRA and isolate the influence of other structures, we conducted a parameter analysis of the modes of antenna II. As shown in Fig. 7(a), when $d = 16.4$ mm, the operating bandwidth of the DRA exhibits four resonant modes. As the height d of the DR increases, it becomes evident that mode III and mode IV gradually shift towards lower frequencies, while the other two modes remain unaltered, with only changes in impedance matching. Fig. 7(b) shows that as the length of the Z-shaped strip increases, the first mode progressively shifts towards lower frequencies, while the mode II remain mostly unchanged. The frequency of mode III and mode IV is slightly shifted downward by the change of strip length. As illustrated in Fig. 7(c), with the gradual augmentation of the rectangular slot's length, only mode II consistently shifts to lower frequencies, while the other three modes remain essentially unaffected. Consequently, this demonstrates that mode I of the antenna corresponds to the strip mode, mode II to the rectangular slot mode, and mode III and mode IV to the degenerate modes of DR.

To ascertain whether the AR frequency band is independently controllable, we conducted a parametric analysis of the strip length and DR height of the proposed antenna. As shown in Fig. 8(a), it becomes evident that as the strip length gradually decreases, the low-frequency passband gradually shifts to higher frequencies, while the high-frequency passband remains mostly unchanged. A similar phenomenon is observed in Fig. 8(b). It is apparent that the two AR passbands can be independently controlled by the strip and the DR respectively. Consequently, the two frequency bands can be flexibly adjusted according to the desired frequency band. At the same time, the radiation nulls play a pivotal role in enhancing the out-of-band selectivity of the DRA. Fig. 9(a) illustrates the effect of spur line length on f_{n2}. Notably, as the spur line length progressively increases, f_{n2} shifts to lower frequencies, while the other two radiating nulls remain unaffected. Similarly, as shown in Fig. 9(b), as the length of the open stub increases, f_{n1} and f_{n3} gradually shift to lower frequencies, while f_{n2} remains unchanged, as expected. Through the parametric investigation of the proposed DBDS CPFDRA, it is evident that different CP frequency bands can be independently controlled by adjusting the Z-shape strip parameters and the DR size, while high out-of-band selectivity can be achieved by modifying the three radiation nulls surrounding the passband.

3. RESULTS AND DISCUSSION

The measurements for the antenna design have been conducted and compared with the simulation results as illustrated in Fig. 10. Within the passband, four modes were identified, encompassing the strip mode (2.54 GHz), slot line mode (2.9 GHz), and a pair of degenerate fundamental modes of DR (3.3, 3.52 GHz). The measured 10 dB impedance bandwidth ($|S_{11}| < -10$ dB) is 38.2% (2.54–3.74 GHz), aligning reasonably well with the simulated values of 39.5% (2.42–3.61 GHz). The overall frequency shift to the high frequency is attributed to the gap introduced between the DR and the dielectric substrate during assembly, as well as the fabrication accuracy of the Z-shaped strip. In the passband, the measured antenna exhibits a flat gain of 4.8 dBi. Notably, the measured realized gain is 0.7 dB lower than the simulation, which is reasonable considering the simulation's omission of the ohmic loss of the strip and coaxial cable. Featuring a radiation null value at 2.2 GHz in the lower band, and two additional radiation nulls at 4.24 GHz and 4.38 GHz in the upper band. As shown in Fig. 10(c), the measured 3 dB AR bandwidths are 2.2% (2.62–2.68 GHz) and 4% (3.44–3.58 GHz) for the lower and upper bands, respectively, catering to the TD-LTE and n78 band. The LHCP gain in low frequency band and RHCP gain in high frequency band were 4.8 and 5.3, respectively.

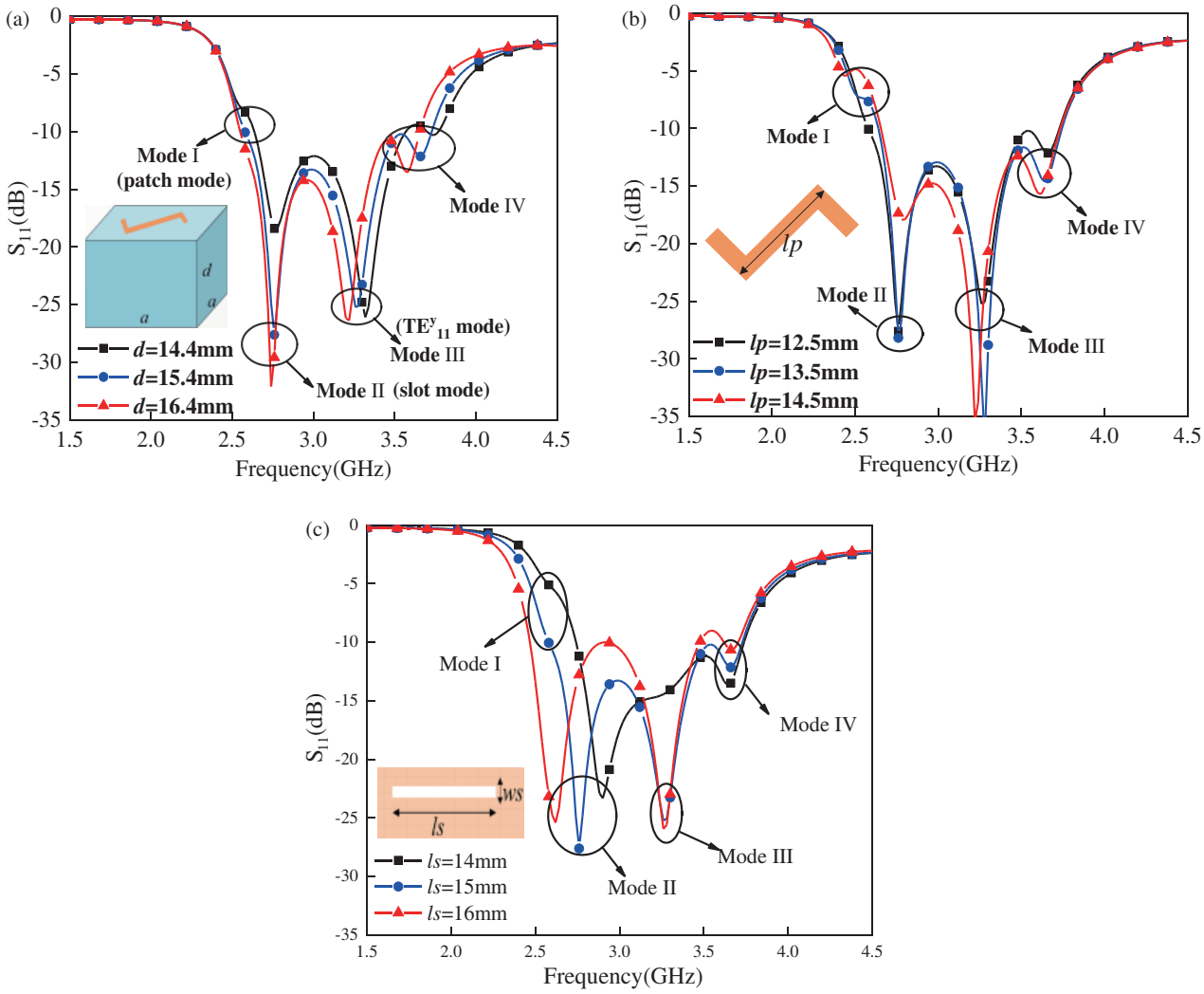

FIGURE 7. Variation of S_{11} with changing (a) d; (b) lp; (c) ls.

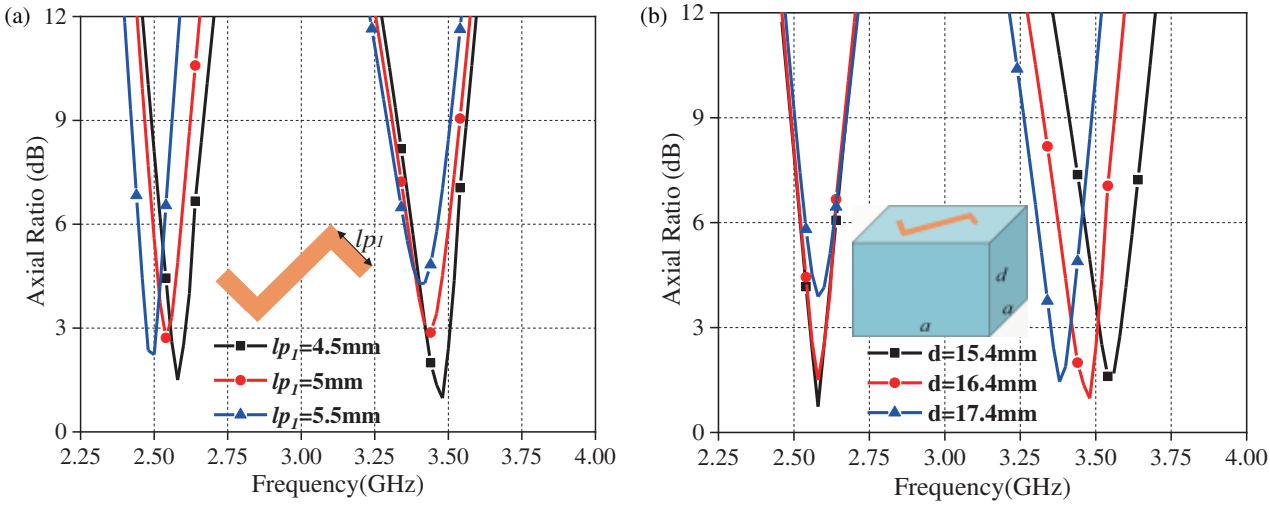

FIGURE 8. Variation of axial ratio with changing. (a) lp_1; (b) d.

Additionally, Fig. 10(d) displays the measured radiation efficiency of the DRA, measuring around 80% in the passband and less than 3% in the stop band. Fig. 11 depicts the radiation pattern of the DRA at the minimum AR value frequencies within the two bands. As observed from the figure, the lower and upper bands radiate LHCP waves and RHCP waves, respectively.

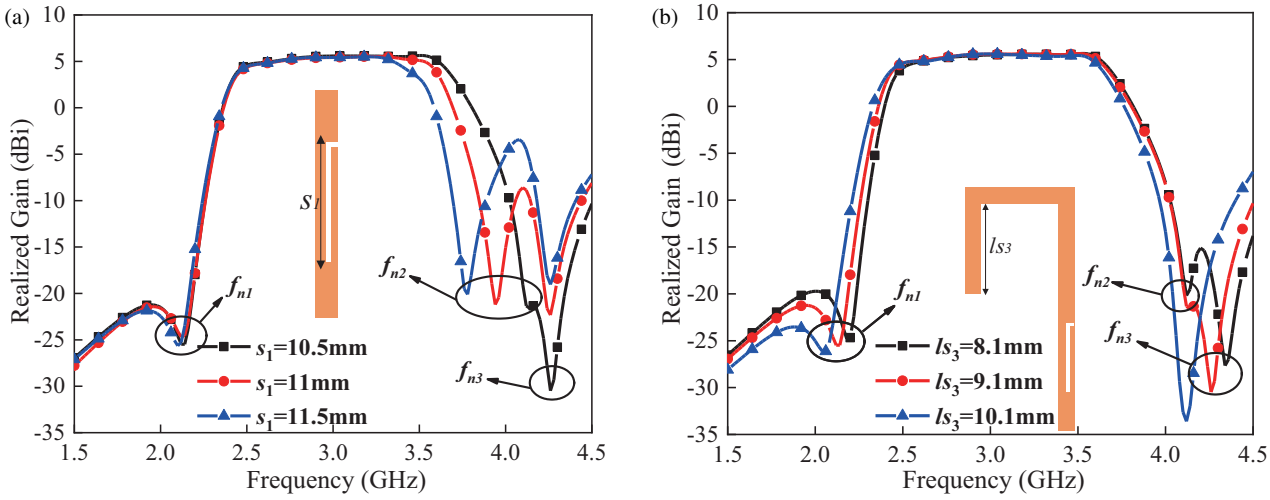

FIGURE 9. Variation of realized gain with changing (a) s_1; (b) ls_3.

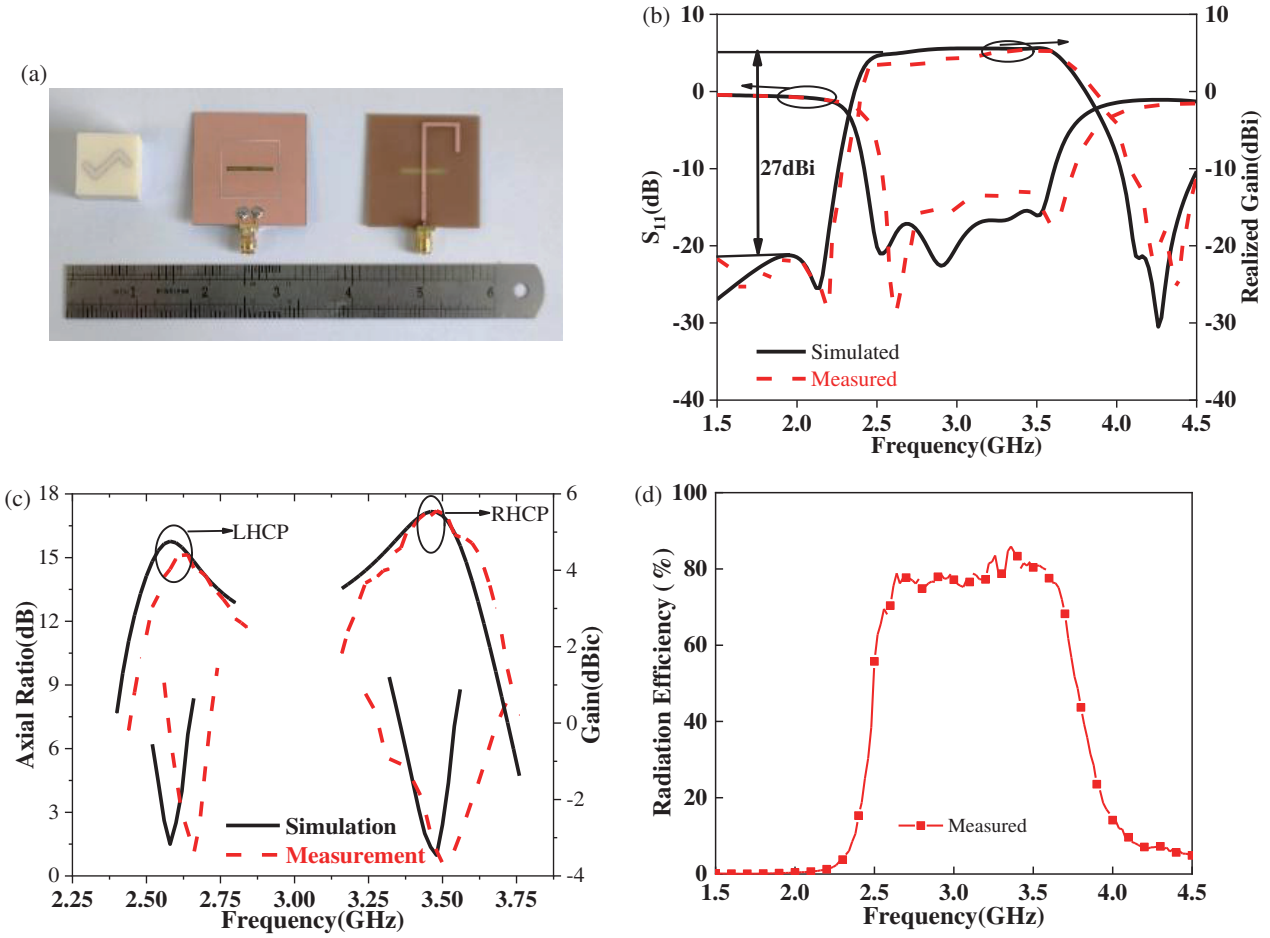

FIGURE 10. (a) View of the manufactured DRA. (b) Simulated and measured S_{11} and Realized Gain. (c) Simulated and measured ARs and radiation gain. (d) Measured radiation efficiencies for the DRA.

The antenna maintains stable performance in the main radiation direction. Notably, the LHCP of the lower band antenna is 17 dB stronger than its RHCP, confirming the lower band antenna's LHCP polarization sense. The RHCP of the upper band is 20 dB stronger than the LHCP, validating the realization of the RHCP.

A comprehensive comparison is presented in Table 2, revealing that the proposed DBDS CPFDRA offers a wider impedance bandwidth, a compact structure, and an indepen-

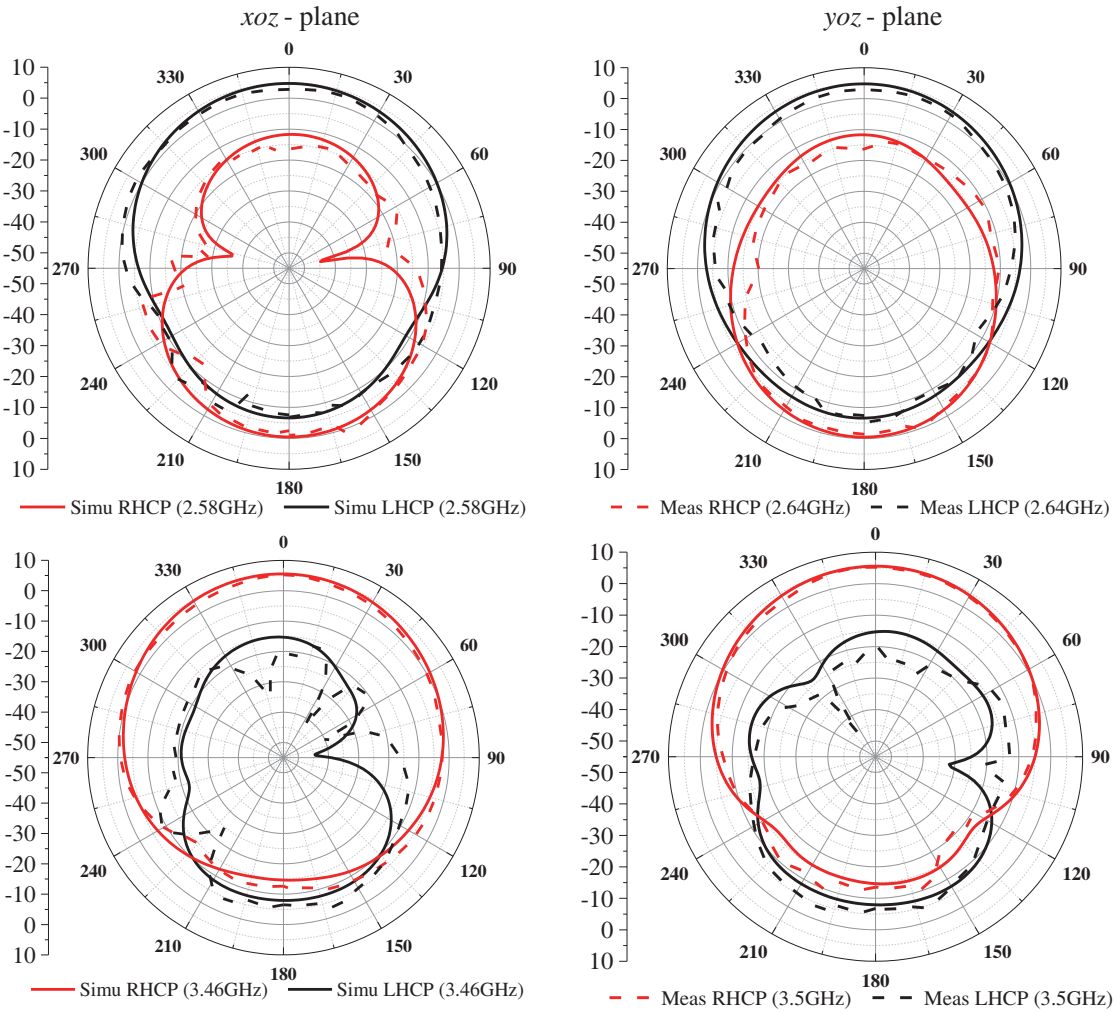

FIGURE 11. Radiation pattern of the DBDS CPFDRA.

TABLE 2. Comparison with the previous antennas.

Ref	Size ($\lambda_0 \times \lambda_0$)	ARBW (%)	Polarization	Number of gain nulls	AR frequency band is IC
Proposed	0.4×0.4	2.2/4	LH/RH	3	Yes
[11]	0.51×0.51	1.5/2.9	LH/RH	Null	No
[12]	0.37×0.37	5.4/10	LH/RH	Null	No
[14]	0.45×0.45	0.6/1.4	LH/RH	Null	No
[15]	2.27×2.27	Null	LP	3	Null
[17]	1.68×1.12	Null	LP	2	Null
[18]	0.81×0.81	4.1	RH	2	No

λ_0: free space wavelength at the center frequency, IC: individually controllable

dently controllable AR bandwidth range. Moreover, owing to the presence of multiple radiation nulls, effective out-of-band selectivity is achieved on both sides of the passband.

4. CONCLUSION

In this paper, we proposed a DBDS CPFDRA with a Z-shaped strip placed on top of the DR. The Z-shaped strip not only served as a perturbation structure to convert the DRA mode of LP field into a CP field at high frequency but also generated CP itself at low frequency, enabling dual-band operation. The lower band is applied in the TD-LTE band, while the upper band was suited for the n78 band for 5G communication. Besides, to achieve miniaturization and multifunctionality, f_{n2} was induced at high frequency through the etching of a spur line on the feedline. To enhance out-of-band suppression at low fre-

quency, f_{n1} was effectively introduced at the lower frequency by intricately designing a half-wavelength open stub beyond the slot line. Additionally, f_{n3} emerged at high frequency due to the frequency doubling effect, thereby improving overall out-of-band selectivity. Finally, we realized a DBDS CPFDRA characterized by a wide bandwidth, flat passband gain, independently controllable AR frequency band, and effective out-of-band suppression, which is a good candidate for 5G wireless communication system applications

ACKNOWLEDGEMENT

This work was supported in part by the National Science Foundation of China under Grant 61661021 and 61901170, in part by the Natural Science Foundation of Jiangxi Province under Grant 20202BABL202008, Department of Education Science and Technology Program of Jiangxi Province under Grant GJJ2200609 and GJJ2200622.

REFERENCES

[1] Li, C., Z.-H. Yan, and W. Hu, "Compact ultra-wideband circularly polarized crossed-dipole antenna with wide angle coverage," *Progress In Electromagnetics Research Letters*, Vol. 111, 85–91, 2023.

[2] Garg, P. and P. Jain, "Isolation improvement of MIMO antenna using a novel flower shaped metamaterial absorber at 5.5 GHz WiMAX band," *IEEE Transactions on Circuits and Systems II: Express Briefs*, Vol. 67, No. 4, 675–679, Apr. 2020.

[3] Wang, K. X. and H. Wong, "A circularly polarized antenna by using rotated-stair dielectric resonator," *IEEE Antennas and Wireless Propagation Letters*, Vol. 14, 787–790, 2015.

[4] Yang, M., Y. Pan, and W. Yang, "A singly fed wideband circularly polarized dielectric resonator antenna," *IEEE Antennas and Wireless Propagation Letters*, Vol. 17, No. 8, 1515–1518, Aug. 2018.

[5] Sharma, A., G. Das, S. Gupta, and R. K. Gangwar, "Quad-band quad-sense circularly polarized dielectric resonator antenna for GPS/CNSS/WLAN/WiMAX applications," *IEEE Antennas and Wireless Propagation Letters*, Vol. 19, No. 3, 403–407, Mar. 2020.

[6] Chakraborty, P., U. Banerjee, A. Saha, and A. Karmakar, "A compact ultra wideband dielectric resonator antenna with dual-band circular polarization characteristics," *International Journal of RF and Microwave Computer-Aided Engineering*, Vol. 31, No. 4, e22577, Apr. 2021.

[7] Sahana, C., N. M. Devi, and M. Jayakumar, "Dual-band circularly polarized annular ring patch antenna for GPS-aided GEO-augmented navigation receivers," *IEEE Antennas and Wireless Propagation Letters*, Vol. 21, No. 9, 1737–1741, Sep. 2022.

[8] Zou, M. and J. Pan, "Wide dual-band circularly polarized stacked rectangular dielectric resonator antenna," *IEEE Antennas and Wireless Propagation Letters*, Vol. 15, 1140–1143, 2016.

[9] Pozar, D. M. and S. M. Duffy, "A dual-band circularly polarized aperture-coupled stacked microstrip antenna for global positioning satellite," *IEEE Transactions on Antennas and Propagation*, Vol. 45, No. 11, 1618–1625, Nov. 1997.

[10] Pan, Y. M., S. Y. Zheng, and W. Li, "Dual-band and dual-sense omnidirectional circularly polarized antenna," *IEEE Antennas and Wireless Propagation Letters*, Vol. 13, 706–709, 2014.

[11] Xu, Y., L. Zhu, N.-W. Liu, and M. Li, "A dual-band dual-circularly-polarized slot antenna with stable in-band gain and reduced frequency ratio under triple resonance," *IEEE Transactions on Antennas and Propagation*, Vol. 70, No. 11, 10 199–10 206, Nov. 2022.

[12] Sharma, A., D. K. Tripathi, G. Das, and R. K. Gangwar, "Novel asymmetrical Swastik-shaped aperture coupled cylindrical dielectric resonator antenna with dual-band and dual-sense circular polarization characteristics," *Microwave and Optical Technology Letters*, Vol. 61, No. 2, 405–411, Feb. 2019.

[13] Zhao, Z., J. Ren, Y. Liu, Z. Zhou, and Y. Yin, "Wideband dual-feed, dual-sense circularly polarized dielectric resonator antenna," *IEEE Transactions on Antennas and Propagation*, Vol. 68, No. 12, 7785–7793, Dec. 2020.

[14] Chen, K., J. Yuan, and X. Luo, "Compact dual-band dual circularly polarised annular-ring patch antenna for BeiDou navigation satellite system application," *IET Microwaves, Antennas & Propagation*, Vol. 11, No. 8, 1079–1085, Jun. 2017.

[15] Liu, H., H. Tian, L. Liu, and L. Feng, "Co-design of wideband filtering dielectric resonator antenna with high gain," *IEEE Transactions on Circuits and Systems II: Express Briefs*, Vol. 69, No. 3, 1064–1068, Mar. 2022.

[16] Wang, C., Z. Han, H. Liu, P. Wen, L. Wang, and X. Zhang, "A novel single-feed filtering dielectric resonator antenna using slot-line stepped-impedance resonator," *IEEE Transactions on Circuits and Systems II: Express Briefs*, Vol. 68, No. 11, 3426–3430, Nov. 2021.

[17] Zhao, C. X., Y. M. Pan, and G. D. Su, "Design of filtering dielectric resonator antenna arrays using simple feeding networks," *IEEE Transactions on Antennas and Propagation*, Vol. 70, No. 8, 7252–7257, Aug. 2022.

[18] Liu, Y.-T., K. W. Leung, J. Ren, and Y.-X. Sun, "Linearly and circularly polarized filtering dielectric resonator antennas," *IEEE Transactions on Antennas and Propagation*, Vol. 67, No. 6, 3629–3640, Jun. 2019.

[19] Jiang, Z. H. and D. H. Werner, "A compact, wideband circularly polarized co-designed filtering antenna and its application for wearable devices with low SAR," *IEEE Transactions on Antennas and Propagation*, Vol. 63, No. 9, 3808–3818, Sep. 2015.

[20] Xiang, B. J., S. Y. Zheng, Y. M. Pan, and Y. X. Li, "Wideband circularly polarized dielectric resonator antenna with bandpass filtering and wide harmonics suppression response," *IEEE Transactions on Antennas and Propagation*, Vol. 65, No. 4, 2096–2101, Apr. 2017.

[21] Luo, W., Y. Feng, Y. Ren, and B. Yin, "A novel wideband fractal rectangular dielectric resonator antenna with improved radiation performance," *AEU-International Journal of Electronics and Communications*, Vol. 142, 153984, 2021.

[22] Zhang, X. and L. Zhu, "Gain-enhanced patch antennas with loading of shorting pins," *IEEE Transactions on Antennas and Propagation*, Vol. 64, No. 8, 3310–3318, Aug. 2016.

[23] Buerkle, A., K. Sarabandi, and H. Mosallaei, "Compact slot and dielectric resonator antenna with dual-resonance, broadband characteristics," *IEEE Transactions on Antennas and Propagation*, Vol. 53, No. 3, 1020–1027, Mar. 2005.